Combustion and Flame 190 (2018) 388–401

Contents lists available at ScienceDirect

Combustion and Flame

journal homepage: www.elsevier.com/locate/combustflame

Constant volume n-Heptane autoignition using One-Dimensional Turbulence

Juan A. Medina M.[a,*], Heiko Schmidt[a], Fabian Mauss[b], Zoltan Jozefik[c]

[a] Brandenburg Technical University Cottbus-Senftenberg, Siemens-Halske-Ring 14, 03046 Cottbus, Germany
[b] Brandenburg Technical University Cottbus-Senftenberg, Siemens-Halske-Ring 8, 03046 Cottbus, Germany
[c] ERC Inc./Air Force Research Lab, Edwards AFB, CA, USA

ARTICLE INFO

Article history:
Received 3 November 2016
Revised 6 February 2017
Accepted 13 December 2017
Available online 6 January 2018

Keywords:
ODT
n-Heptane
Autoignition
DNS
Ensemble

ABSTRACT

Constant volume premixed lean n-Heptane/air autoignition at high pressure is investigated using the One-Dimensional Turbulence (ODT) model. The configuration consists of a 1D fixed volume domain with a prescribed velocity spectrum and temperature fluctuations superimposed on an initial uniformly elevated scalar field. The sensitivity of the heat release rate and pressure evolution to the initial temperature distribution is studied by imposing different initial temperature fields while holding the mean, RMS and integral length scale of the field constant. Three detailed chemical mechanisms are employed for the prediction of autoignition and heat release rate. To mitigate the high computational cost associated with the calculation of the chemical source terms in the stiff complex mechanisms, an approach based on the Strang-Splitting method is presented. Finally, a study of the ODT model uncertainty is carried out. For validation, ODT results are compared to 2D DNS data from Yoo et al. (2011) for the temporal evolution of heat release rate, pressure and density-weighted displacement speed. Ensemble averaged ODT results show good agreement with the DNS data. ODT results generated from varying the initial temperature fields show that the ignition delay time is highly sensitive to the initial temperature field. The ODT model uncertainty study shows that dispersion due to the stochastic nature of the model is considerably smaller than the dispersion resulting from varying the initial temperature field. Overall, this study demonstrates that ODT accurately captures the evolution of complex chemistry reactive flows in constant volume autoignition simulations and that once validated, ODT is an efficient tool that can be used to carry out parametric studies not feasible by DNS.

1. Introduction

The volumetric energy density of fossil fuels in the energy transport sector has led to their dominance over emerging, alternative fuels in the field. Among the different types of fossil fuels, the characterization of n-Heptane as a surrogate fuel for Diesel takes strategic importance, mainly due to the wide range of operational conditions over which it can be used. In this context, there has been a significant amount of time and effort in combustion research devoted to the topic of Homogeneous Charge Compression Ignition (HCCI) engines. HCCI engines have shown that very low emissions and high fuel efficiency values are feasible through constant volume autoignition.

Several Direct Numerical Simulation (DNS) studies have been focused on the topic of constant volume autoignition [1–7]. Within the DNS research, the study of constant volume autoignition has led not only to the understanding of interesting fundamental phenomena, well detailed in the work of Yoo et al. [5], but it has also symbolized the achievement of major milestones in terms of computational power. A pioneering 2D DNS that considered inhomogeneous scalar fields was performed with reduced hydrogen/air chemistry by Sankaran et al. [4], and a follow-up study with a wider range of initial conditions was carried out by Chen et al. [2]. The latter study allowed a clearer characterization of deflagration and detonation regimes during constant volume autoignition processes. The study was also chosen as a test case for the Linear Eddy Modeling (LEM) approach in constant volume autoignition, discussed by Oevermann et al. [8].

It was not, however, until 2011 that increased computational power and a series of chemistry reduction methods allowed the first 2D DNS simulation for a n-Heptane/air mixture by Yoo et al. [5]. This work showed that RMS temperature fluctuations have a first-order effect on the ignition characteristics of n-Heptane/air

* Corresponding author.
E-mail address: medinjua@b-tu.de (J.A. Medina M.).

https://doi.org/10.1016/j.combustflame.2017.12.015
0010-2180/

mixtures. In 2013, another milestone was achieved by Yu and Bai [6], who conducted the first 3-D DNS of a constant volume autoignition environment with a premixed hydrogen/air gas mixture. The work by Yu and Bai [6] is pioneering in the sense that a first insight was given to the turbulence dynamics within autoignition, e.g. by studying the Turbulent Kinetic Energy (TKE) evolution prior to ignition.

Despite the robustness of the LEM results [8] previously cited, the findings in [6] show the importance of the evolution of the turbulent state of the flow on the ignition characteristics. Such influences cannot be obtained in LEM due to the inherent limitations of the model. This is the reason why the One-Dimensional Turbulence (ODT) model gains importance in this case.

In essence, as a stand-alone model, ODT belongs to the family of stochastic turbulence models. ODT does not model small scale phenomena, but as in DNS, it is directly resolved. In contrast to DNS, however, 3-D Navier–Stokes turbulence is modeled via a solution dependent sequence of stochastic 1-D events. ODT preserves many characteristics of LEM, but additionally features an intrinsic dynamic feedback between the turbulent fluctuations and the average state of the flow [9].

Recent ODT studies followed DNS research by gradually increasing the complexity of the benchmark cases. Jozefik et al. [10] considered a variable density formulation for ODT in a constant volume autoignition process as a benchmark test for the introduction of the Darrieus–Landau instability model. Building upon this, the compressible ODT formulation in [11] followed. For an application-relevant fuel like n-Heptane, the computational savings of ODT in comparison to DNS could allow important insights regarding the behavior of the fuel in complex operating conditions such as constant volume autoignition processes. With this work, the authors present the first framework for the treatment of stiff chemistry for such processes within ODT. As a stepping stone from the previous LEM study, this work is also focused on the influence of temperature inhomogeneities in the initial highly reactive mixture.

This paper is organized as follows. Section 2 provides the modeling approach. Specifically, Section 2.1 presents the numerical formulation, Section 2.2 gives a short overview of ODT, Section 2.3 introduces the ODT constant volume configuration specific models, Section 2.4 describes the Strang-Splitting method and the numerical time advancement, and Section 2.5 discusses the mesh adaption procedure. In Section 3, details concerning the configuration are given and in Section 4, ODT results are compared to DNS data for the temporal evolution of heat release rate, pressure and density-weighted displacement speed. These results are discussed from the point of view of the influence of randomized initial conditions in Section 4.1, the sensitivity to the ODT model parameters in Section 4.2, and the influence of the magnitude of the temperature inhomogeneities in Section 4.3. The sensitivity of the simulations to the initial conditions is also compared to the uncertainty of the ODT model (due to the 1-D stochastic events). An additional sensitivity analysis linked to the reaction chemistry is also presented. Concluding remarks are provided in Section 5. In Appendix A, details of the velocity evolution in ODT are given and in Appendix B, a convergence analysis of the time-stepping scheme is shown.

2. ODT model formulation

2.1. Conservation equations for the diffusion–reaction system

Due to the one-dimensional modeling of multi-dimensional turbulence interactions in ODT, the generalized Navier–Stokes equations are not solved by the model. Rather, a set of diffusion–reaction evolution equations coupled to instantaneous implementation of stochastic 1-D eddy events is considered. The main idea behind the ODT modeling is the separate treatment of the diffusion/reaction processes from the turbulent advection. As such, the structure of the theoretical and modeling background in this paper will also separately address these two components of ODT.

Although previous work done by Jozefik et al. [11] introduced a compressible formulation for ODT, the stiffness of the chemistry employed in this study forced the authors to opt for the simpler Zero-Mach classical ODT formulation, which has been the subject of numerous publications in the field of reactive flows (see e.g. [12–14]). In terms of comparison to the DNS from Yoo et al. [5], only relatively large values of initial RMS temperature fluctuations are evaluated in this paper. According to Yoo et al. [5], these large initial RMS temperature fluctuations values translate into deflagration-dominated regimes with a characteristic low subsonic displacement speed. This guarantees the validity of the Zero-Mach limit approximation.

The details of the diffusion–reaction evolution equations are given here considering a Lagrangian formulation of the conservation equations, similar to the framework in [15]. The conservation of properties in each of the control volumes in the one-dimensional domain is given by the application of the Reynolds Transport Theorem (RTT) to a Lagrangian system intensive property β,

$$\frac{d}{dt}\int_{\forall_{(t)}} \rho\beta d\forall = \frac{\partial}{\partial t}\int_{CV} \rho\beta d\forall + \oint_{CS} \rho\beta(\vec{V}-\vec{V}_{CV})\cdot d\vec{S}. \tag{1}$$

In Eq. (1), CS refers to the boundary of the Control Volume (CV), ρ is the density of the Lagrangian system and $\forall$ represents the Lagrangian system volume. If the velocities of the equivalent moving CV are assumed to be equal to the Lagrangian system velocities, $\vec{V}_{CV} = \vec{V} = u_{L,j}$, then it is possible to omit the last term on the Right-Hand Side (RHS) of Eq. (1). We use $u_{L,j}$ to refer to the three components of the Lagrangian system velocity. These are not equivalent to the three velocity components normally solved in ODT, u_j. Details of the relation between the ODT velocity components u_j and the Lagrangian velocities $u_{L,j}$, which comply with Eq. (1), can be found in Section 2.3.

In the Zero-Mach number limit combustion, the velocity field admits an orthogonal decomposition into zero-divergence and non-zero-divergence contributions [16]. Similar considerations can be applied to the diffusion–reaction evolution of the Lagrangian velocity field considered here. We define our system of equations for Zero-Mach combustion as one comprised by the variables of thermodynamic pressure P, the Lagrangian velocity field $u_{L,j}$, the species mass fractions present in the gas mixture Y_k and the enthalpy of the mixture h. Such a system of equations, in terms of non-conservative variables, implies conservation of mass, i.e. the density evolution Partial Differential Equation (PDE) can be derived from such a system of equations, although it does not need to be resolved directly [16]. The system of equations comprises then a PDE for momentum conservation acting over a zero-divergence velocity contribution for $u_{L,j}$, species mass fractions and enthalpy PDEs, an expression for the temporal rate of change of the pressure, as well as the non-zero divergence condition for the complementary contribution to $u_{L,j}$.

The momentum equation evolution is used in ODT as a mechanism to update the velocity components influencing the selection of eddy events, i.e., the ODT velocity components u_j experiencing diffusion evolution and influencing turbulent advection (see Section 2.2). u_j velocity components comprise the divergence-free part of $u_{L,j}$. The formulation for the momentum equation in this work follows then the original incompressible ODT momentum evolution in [15], derived from the RTT, Eq. (1),

$$\rho\frac{\partial u_j}{\partial t} = \frac{\partial}{\partial x}\left(\mu\frac{\partial u_j}{\partial x}\right), \tag{2}$$

where μ is the dynamic viscosity of the flow. Note that all the equations from [15] are written in this work, for simplicity, in a differential form, but they are the same as those reported in the original work.

The conservation equations for species and enthalpy are also obtained by application of the RTT, Eq. (1) [15]. Modeling the species diffusion velocities by the Hirschfelder and Curtis' approximation [17], the correspondent enthalpy and species equations are respectively

$$\rho\frac{\partial Y_k}{\partial t}=\frac{\partial}{\partial x}\left(\rho D_k\frac{\partial Y_k}{\partial x}+\frac{\rho D_k Y_k}{M}\frac{\partial M}{\partial x}\right)+\dot{w}_k, \tag{3}$$

$$\rho\frac{\partial h}{\partial t}=\frac{dP}{dt}+\frac{\partial}{\partial x}\left(\lambda\frac{\partial T}{\partial x}\right)+\frac{\partial}{\partial x}\left[\sum_{k=1}^{N}\left(h_k\frac{\rho D_k Y_k}{X_k}\frac{\partial X_k}{\partial x}\right)\right]. \tag{4}$$

Here P is the leading order thermodynamic pressure, D_k is the kth species mixture-averaged diffusion coefficient and Y_k, X_k correspond to the kth species mass and mole fractions respectively. M is the mean molecular weight of the mixture, $\dot{w}_k$ is the kth species reaction rate and h_k is the kth species enthalpy (including the enthalpy of formation). The rest of the symbols, T, ρ and h correspond to the local temperature, density and enthalpy of the mixture respectively. The equation of state for a mixture of ideal gases is, in this case

$$P=\frac{\rho TR}{M}, \tag{5}$$

being R the universal gas constant.

The non-zero divergence condition in the Zero-Mach combustion is linked to the complementary contribution to $u_{L,j}$, i.e. a deformation (or dilatation) velocity field $u_{D,j}$ (the reader is advised to refer to the derivation of Eq. (28) in [15]). For a 1-D domain, this is

$$\frac{\partial u_{D,1}}{\partial x}=-\frac{1}{\gamma P}\frac{dP}{dt}+Q. \tag{6}$$

where $u_{D,1}$ is the dilatation velocity associated with the density changes in x direction, and γ is the ratio of specific heats. Q is given by

$$Q=\frac{1}{\rho c_p T}\left\{\frac{\partial}{\partial x}\left(\lambda\frac{\partial T}{\partial x}\right)+\sum_{k=1}^{N}\left[h_k\left(\frac{\partial}{\partial x}(\rho V_k Y_k)-\dot{w}_k\right)\right]\right\}$$
$$-\frac{M}{\rho}\sum_{k=1}^{N}\left\{\frac{1}{M_k}\left[\frac{\partial}{\partial x}(\rho V_k Y_k)-\dot{w}_k\right]\right\}, \tag{7}$$

where M_k is the molecular weight of species k, and V_k is a shorthand notation for the k-species diffusion velocities, which in the case of the Hirschfelder and Curtis' approximation used in this model takes the form

$$V_k=-D_k\frac{\nabla X_k}{X_k}=-D_k\left(\frac{1}{Y_k}\nabla Y_k+\frac{1}{M}\nabla M\right). \tag{8}$$

Finally, it is also possible to derive an expression for the temporal change of pressure by integrating Eq. (6) over the domain of length L, noting the spatially uniform thermodynamic pressure. This derivation can also be found in [15],

$$\frac{dP}{dt}=\left[(u_{D,x=L}-u_{D,x=0})-\int_{x=0}^{x=L}Q\,dx\right]\frac{-P}{\int_{x=0}^{x=L}\frac{1}{\gamma}dx}. \tag{9}$$

2.2. ODT turbulent advection modeling

The turbulent advection of the flow is modeled in ODT as a sequence of intermittent eddy events, which preserve mass, momentum and energy. Eddy events symbolize the coupling between the chemical and turbulent flow state. They modify the scalar profiles corresponding to the conserved flow properties, and simultaneously influence the determination of future eddy events.

Each eddy event in ODT is characterized by three parameters, namely, the eddy location x_0, the eddy size l and the eddy rate λ. An eddy event consists of a map that mimics the stirring of property profiles. This is done in ODT by means of the triplet map [9]. Scalar profiles are only subject to eddy stirring effects and thus need only be mapped. Additional constraints arise for the velocity profiles, which need to be mapped but must also comply simultaneously with an overall total kinetic energy conservation among the three velocity components of the velocity field [18]. Therefore, an additional Kernel function is applied in order to enforce these criteria and redistribute energy among the three velocity components. Energy redistribution is associated to the parameter α [18], which in this work was assumed to take the standard value $\alpha=2/3$, implying equal energy redistribution among the three velocity components.

The triplet map operation is a transformation rule for the position of the discrete elements of the scalar and velocity profiles within the interval $[x_0, x_0+l]$, at a certain instant of time determined by the eddy rate λ. The positions are mapped onto three subintervals according to a three-valued function of x

$$f(x;x_0,l)=\begin{cases}x_0+f_1(x-x_0), & x_0\le x\le x_0+f_1 l\\ x_0+f_2 l-(f_2-f_1)(x-x_0), & x_0+f_1 l\le x\le x_0+f_2 l.\\ x_0+f_2 l+(1-f_2)(x-x_0), & x_0+f_2 l\le x\le x_0+l\end{cases} \tag{10}$$

Eq. (10) maps the interval $[x_0, x_0+l]$ onto each of three subintervals $[x_0,\ x_0+f_1 l]$, $[x_0+f_1 l,\ x_0+f_2 l]$ and $[x_0+f_2 l,\ x_0+l]$, where $f_1=1/3$ and $f_2=2/3$ [9].

The eddy location x_0 is sampled from a uniform distribution over the full ODT domain. The eddy size l is selected from an eddy-size PDF that comprises eddies between the Kolmogorov length-scale and the full domain length. The eddy rate λ is calculated on the basis of a dimensional analysis, and is related to the eddy turnover time τ and the square of the eddy size l. Details of the statistical eddy sampling and selection can be found in [19].

τ can be modeled from the kinetic energy expression for an eddy $E_{kin}=0.5\rho\forall v^2$, with the eddy velocity v expressed as l/τ, i.e. $E_{kin}=0.5\rho l(l/\tau)^2$. This is the basis of the dimensional modeling of the eddy turnover time and thus, leads to the expression found in [14]

$$\frac{1}{\tau}=C\left[\frac{2K_0}{\rho_0 l^3}(E_{kin}-ZE_{vp}+E_{pe})\right]^{1/2}. \tag{11}$$

Here C is a proportionality constant affecting the eddy rate, i.e. C represents the intensity of the turbulence and is an ODT model parameter that needs to be calibrated. Z is normally determined to be an order-unity parameter of the ODT model, which nonetheless, needs to be calibrated [19]. Also, $K_0=\int K^2dx$ and $\rho_0=\int\rho K^2dx$, where K is a Kernel function in ODT [19].

The additional energy terms in Eq. (11) are the potential energy change (E_{pe}) due to the instability caused by the eddy implementation in the variable density flame front [14], as well as an energy penalty (ZE_{vp}) that reflects viscous dissipation effects [19]. If these terms are neglected, then the original dimensional relation between E_{kin} and τ is recovered. However, due to the modeling used in this work, both terms are retained for the calculation of the turnover time. A detailed discussion concerning the energy terms in Eq. (11) along with their calculation method can be found in [19]. Guidelines for the case-specific term E_{pe} can be found in Section 2.3.

One final aspect worth noting regarding the ODT turbulent advection modeling, is that the use of the eddy-size PDF for the selection of l can result in the selection of eddies that are unphysi-

cally large [18]. A discussion of possible mechanisms for large eddy suppression can be found in [19]. We do not apply any kind of suppression mechanism for the eddies in this work. Instead, eddies are implemented only in the range between the computed Kolmogorov length-scale η_K corresponding to the given initial conditions, and the DNS integral length-scale l_t. The Kolmogorov length-scale η_K is computed following the relation between the turbulent Reynolds number (Re_t) based on the DNS integral length-scale, and the well-known relation $\eta_K/l_t = Re_t^{3/4}$.

2.3. Constant volume autoignition modeling

Modeling considerations are required for non-canonical cases in ODT. Although it is not strictly part of the modeling, we discuss in this section the treatment of the thermodynamic pressure P. Despite having its own evolution equation, P is not updated in this work using Eq. (9). Eq. (9) is only used in this work to evaluate the dP/dt term used for enthalpy time-advancement in Eq. (4). However, the resulting pressure after the advancement of the chemical system given by h and Y_k at constant volume does not need to be calculated by time-advancement. Rather, it can be evaluated by means of the ideal gas law applied to the closed computational domain. This is a direct analogy of the methodology used in [20],

$$P = \frac{R\left(\int_{x=0}^{x=L} \rho dx\right)_{t=0}}{\int_{x=0}^{x=L} \left(T \sum_k \frac{Y_k}{M_k}\right)^{-1} dx}. \tag{12}$$

The integral expression in the numerator of the fraction corresponds to the initial mass of the system, which is conserved during the simulation. The length of the domain is also assumed to remain constant.

For the study case considered here, the Lagrangian velocities $u_{L,j}$ used in the RTT equation, Eq. (1), and applied to the set of conservation equations discussed in Section 2.1, are made up of the sum of the advective and deformation (dilatation) velocities. I.e., these are the sum of density-related and density-unrelated contributions to the velocity vector. This is the previously mentioned velocity field decomposition and follows a similar philosophy to the modeling suggested in [14]

$$u_{L,j\ (\text{Lagrangian})} = u_{j,\ (\text{net advection = turbulent advection})} + u_{D,j\ (\text{deformation})}. \tag{13}$$

In comparison to [14], however, the net advection of the system is given in this case only by the turbulent advection modeled by ODT, due to the zero mean advection contribution in constant volume systems. The position of the individual control volumes, which corresponds to that of the Lagrangian system (zero relative-velocity), is then determined from the velocity components $u_{L,j}$. Further discussion regarding the evolution of these Lagrangian velocity components can be found in Appendix A.

Starting from Eq. (13), it can be shown that the position of the individual Control Volumes is influenced by the correspondent volume of the cells and the turbulent transport. Even though the mean density of the system remains unchanged due to the constant mass and volume during the time evolution, local volume (and density) changes are expected according to Eq. (6). These changes translate into the spatially uniform increase of the thermodynamic pressure given by Eq. (9). For this study, all of the dilatation of the system is assumed to be confined to the ODT line (no flow is assumed to leave the line). Here, $u_{D,1} = u_D$ and $u_{D,2} = u_{D,3} = 0$ in Eq. (13). In the absence of eddy events, during the sole diffusion–reaction evolution, this dilatation follows from the implied continuity equation,

$$\frac{D\rho}{Dt} + \rho \frac{\partial u_D}{\partial x} = 0. \tag{14}$$

Following from this, in 1-D with mass and volume conservation within the ODT line, the dilatation velocity u_D is equal to the definition of the velocity by means of the displacement of the cells faces

$$u_D = \frac{dx}{dt}. \tag{15}$$

Thus, the two methods for the calculation of u_D, Eqs. (14) and (15), are equivalent and consistent with the formulation. We use the second approach in this work.

In order to account for the influence of the dilatational flow on the eddies, the Darrieus–Landau instability model was introduced [14]. The effect is formally incorporated into the E_{pe} energy term required for the calculation of the eddy turnover time in Eq. (11)

$$E_{pe} = \frac{8}{27} \int_{x_0}^{x_0+l} a_{(x)} K_{(x)} \left(\rho_{[f(x;x_0,l)]} - \overline{\rho}\right) dx, \tag{16}$$

where the Kernel definition $K = f(x; x_0, l) - x$ was used [19]. $\overline{\rho}$ corresponds to the average density over the sampled eddy length, while a is the acceleration induced by the variable density flame-front. For further details and considerations regarding this energy term, the reader is referred to Jozefik et al. [14].

For this work, the acceleration term a in Eq. (16) is given simply by the temporal change of the dilatational velocity

$$a = \frac{\partial u_D}{\partial t}. \tag{17}$$

2.4. Numerical advancement of the stiff diffusion–reaction system

Previous studies in LEM and ODT have used different strategies to handel stiff chemistry time integration (see e.g. [15] and [21]). During the initial phase of this study, these approaches were applied to the current test cases and resulted in extremely small time-steps in order to achieve stable solutions ($\Delta t_{req} << 1 \times 10^{-9}$s). Such small time-steps result in extremely costly simulations. Thus, an alternative approach was implemented in order to improve efficiency. The alternative approach is based on the operator Strang-Splitting method developed in [22]. This approach was able to remedy the time-step limitations, such that values of $\Delta t_{req} > 1 \times 10^{-9}$s could be achieved.

Before proceeding, the reader is advised that all of the equations reported here are solved by means of a FVM discretization scheme as in [15]. The advancement of the governing equations is given by the splitted treatment of the diffusion and reaction operators. First, the chemical subsystem is advanced considering the splitting approach in the species and enthalpy evolution equations, Eqs. (3) and (4), respectively. The diffusive advancement over one half of the time step integrates the subsystem:

$$\rho \frac{\partial Y_k}{\partial t} = \frac{\partial}{\partial x}\left(\rho D_k \frac{\partial Y_k}{\partial x} + \frac{\rho D_k Y_k}{M} \frac{\partial M}{\partial x}\right), \tag{18}$$

$$\rho \frac{\partial h}{\partial t} = \frac{\partial}{\partial x}\left(\lambda \frac{\partial T}{\partial x}\right) + \frac{\partial}{\partial x}\left[\sum_{k=1}^{N} \left(h_k \frac{\rho D_k Y_k}{X_k} \frac{\partial X_k}{\partial x}\right)\right]. \tag{19}$$

The species diffusion equation, Eq. (18) is advanced with a second-order Crank–Nicolson discretization scheme, over a time step $\Delta t/2$. The enthalpy equation is advanced with a second-order explicit Runge–Kutta predictor–corrector method. This avoids the formulation of an excessively complex implicit matrix to treat Eq. (19). The species mass fractions values at time step $\Delta t/4$ required for the corrector step of the enthalpy equation are obtained from an additional advancement of the species PDE (using the same Crank–Nicolson method for simplicity). Once the values of the species and enthalpy are available at the time level $\Delta t/2$, the reaction part of

the splitting can be calculated with the chemical subsystem

$$\rho \frac{\partial Y_k}{\partial t} = \dot{w}_k, \tag{20}$$

$$\rho \frac{\partial h}{\partial t} = \frac{dP}{dt}. \tag{21}$$

The temporal advancement of Eqs. (20) and (21) is done over a time step Δt. In order to advance the enthalpy reaction equation, Eq. (21), the thermodynamic pressure local change must be calculated by means of Eq. (9), using the information obtained at the end of the diffusion sub-step. The species reaction equation, Eq. (20) is solved implicitly at constant enthalpy by means of a Newton-Method iteration. In practice, this is done by CVODE [23]. The enthalpy reaction equation, Eq. (21) is solved by a first order explicit Euler method.

To finalize the advancement of the chemical system, another diffusive advancement over $\Delta t/2$ is done, exactly as in the first diffusion step. At all times during the operator splitting, the density of the mixture is assumed to remain constant. The resulting thermodynamic pressure at the end of the splitting approach is calculated from Eq. (12), using the updated values of h and Y_k (T is calculated as a function of h and Y_k at constant volume and pressure). Thermodynamic and transport properties are calculated using the C++ interface of the Cantera software package [24]. The density update in the new time step can be found afterwards by means of the ideal gas law (solved by Cantera), considering the calculated species mass fractions, enthalpy and pressure after the operator splitting procedure.

The implicit advancement of the discretized momentum equation, Eq. (2), is done after the full advancement of the chemical system. In this work, the ODT velocity components u_j were obtained by means of a first-order implicit Euler approximation.

In order to account for the dilatational velocities u_D influencing the eddy events and simultaneously enforce the non-zero divergence condition, new cell sizes satisfying Eq. (6) are calculated. In order to carry out the calculation, Eq. (15) is discretized and substituted into Eq. (6)

$$\left[\left(-\frac{1}{\gamma P}\frac{dP}{dt} + Q\right)_i^{n+1} \Delta x_i^n\right]\Delta t = \Delta x_i^{n+1} - \Delta x_i^n. \tag{22}$$

Here, Δx_i indicates the cell size at position i and the superscripts $n, n+1$ indicate the correspondent time steps. The divergence condition is evaluated with the values obtained at time step $n+1$. This ensures the enforcement of the Boundary Conditions for u_D and allows its direct calculation for its use in the evaluation of the eddy turnover time, Eq. (11).

Due to the combination of different numerical schemes that typically lead to time-splitting errors during numerical integration, a brief study commenting the overall precision of the scheme and its numerical convergence can be found in Appendix B.

2.5. Adaptive ODT formulation

The version of the ODT code used for this work incorporates the mesh adaption technique discussed in Lignell et al. [15]. This technique is based on the distribution of cells in a certain region of the domain considering equal arc lengths of the property profiles between pairs of cells. The properties used to determine the arc lengths in the re-assignment of cells within the region to adapt are selected prior to the simulation. In this work, all of the time-evolving properties were selected as critical parameters of the adaption function.

The re-distribution of the cells within the region to adapt considers a grid density factor that determines the new number of cells to create in the adapted region, and which will determine the interpolated properties profiles in the new mesh. This grid density factor is a user specified parameter gDens. Additionally, the mesh adaption procedure takes as an input the minimum and maximum cell size to be created during the mesh refinement. The minimum cell size is determined in order to have a proper resolution of the expected smallest physical length scales that need to be resolved in the simulation. The maximum cell size should be considered as a parameter sufficiently larger than the minimum cell size to speed up the simulation, but not so large as to provoke numerical artefacts.

Table 1
ODT initial conditions and parameter settings.

Parameter	Value
Initial mean temperature, T_0 (K)	934
Initial mean pressure, P_0 (atm)	40
Initial fuel-air equivalence ratio Φ	0.3
Initial laminar burning velocity s_L (m/s)	0.36
Initial isotropic velocity fluctuations v' (m/s)	0.5
Initial turbulent Reynolds number $Re_t = v' l_t/\nu$	220
Domain length X_{ODT} (m)	3.2×10^{-3}
Integral Eddy length scale l_t (m)	1.24×10^{-3}
Initial number of cells	640
Minimum cell size (mesh adaption function) dxmin (m)	4.16×10^{-6}
Maximum cell size (mesh adaption function) dxmax (m)	3.2×10^{-5}
Grid density factor (mesh adaption function) gDens	80.0

The user-specified input parameters of the mesh adaption function, gDens, dxmin (minimum cell size allowed) and dxmax (maximum cell size) can be found in Table 1 for all of the simulation results obtained in this work. The mesh input parameters are selected in a way as to obtain mesh-independent results.

3. Simulation setup

3.1. Flow configuration, boundary and initial conditions

The selected flow configuration corresponds to the one-dimensional representation of the 2-D DNS [5] square domain. Since ODT represents a line of sight through the turbulent flow within the 2-D domain, as in the DNS, periodic boundary conditions are applied to the ODT line. The length of the ODT line (domain length) corresponds to the side length of the square DNS domain.

Initial conditions for the pseudo-homogeneous initial mixture field are given by the definition of the velocity, species mass fractions, temperature and pressure spatial profiles at $t = 0$.

- Species mass fractions profiles are initialized at a constant Air–Fuel equivalence ratio.
- The ODT velocities u_j are initialized by a Passot–Pouquet turbulence spectrum in analogy to [8], that is

$$E(k) = \frac{32}{3}\left(\frac{2}{\pi}\right)^{1/2}\frac{v'^2}{k_e}\left(\frac{k}{k_e}\right)^4 \exp\left[-2\left(\frac{k}{k_e}\right)^2\right]. \tag{23}$$

Here, k is the wave number, k_e is the most energetic wave number defined by $k_e = 2\pi/l_t$ and v' is the RMS velocity fluctuation. The integral length scale l_t is assumed in this case to be equal in magnitude to the most energetic length scale. The resulting initial velocity field $v(x)$, which is used to initialize each one of the ODT velocity components u_j is

$$v(x) = v_0 + \sum_{k=1}^{K} (\Delta v)_k \sin(2\pi kx/l_t + \phi_k). \tag{24}$$

where $K \to \infty$, v_0 denotes the initial mean velocity field and ϕ_k is the randomly chosen phase of the kth wave with $0 \le \phi_k \le 2\pi$.

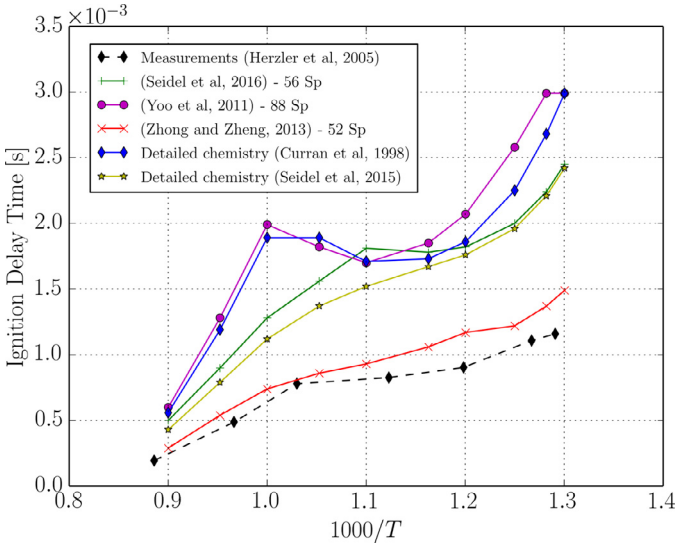

Fig. 1. Ignition Delay Times (IDT) for 0-D homogeneous reactor. Comparison of the preselected chemical mechanisms to experiments. Detailed chemistry mechanisms results are shown as well for reference.

The velocity amplitude at wavenumber k for a periodic velocity field (initially isotropic) Δv, is given by

$$(\Delta v)_k \approx [2E(k)]^{1/2} \tag{25}$$

- The temperature profile is defined similarly as in Eqs. (23)–(25), by means of a Passot–Pouquet spectrum. Only sufficiently large values of RMS temperature fluctuations T' are used for initialization ($T' = 60$ K, 100 K). This similar initialization of the temperature and velocity fields is done following the methodology of the DNS study used for comparison [5]. As in the DNS, both fields are initialized with different random numbers in order to ensure that they are not correlated.
- The pressure P is initialized spatially uniform with P_0.

A summary of the initial conditions is given in Table 1. For the first part of this work, we consider initial RMS temperature fluctuations of $T' = 60$ K. After calibrating the ODT parameters, an exploratory study is done with a temperature fluctuation of $T' = 100$ K, analogous to [5].

3.2. Pre-selection of the chemical mechanisms

Three different chemical mechanisms are used in this work. Since the initial conditions of the DNS imply the use of the Low Temperature Chemistry (LTC) regime for n-Heptane, a preliminary 0-D homogeneous validation for the set of available chemical mechanisms was carried out. We compared the results of the Ignition Delay Times (IDT) to those obtained experimentally by Herzler et al. [25] at conditions of $P_0 = 50$ atm, $T_0 = 934$ K, $\Phi = 0.3$. Note that even though the DNS was carried out at $P_0 = 40$ atm, the 0-D homogeneous reactor validation is carried out at $P_0 = 50$ atm due to the non-availability of experimental results at $P_0 = 40$ atm. Despite the differences in the values of the initial homogeneous pressure, the results are expected to offer a sufficiently good framework for comparison of IDTs.

Results of the 0-D homogeneous reactor validation are shown in Fig. 1. Note that only the physically coherent mechanisms results are shown. Mechanisms not shown here exhibited unphysical behavior regarding the IDTs at the specified initial conditions. The obtained IDTs at $P_0 = 50$ atm, $T_0 = 934$ K, $\Phi = 0.3$ for the mechanisms of Seidel et al. [26], Yoo et al. [5] (88 species) and Zhong and Zheng [27] are sufficiently close to the experimental values obtained in [25] as to validate the preselection. Although the 0-D homogeneous behavior from the mechanism of Zhong and Zheng [27] is closer to the experimental IDTs, it shows a multi-stage ignition process in the temporal evolution of the heat release rate, i.e. the presence of two peaks in the heat release rate evolution (not shown here). A similar behavior is obtained for the mechanism of Seidel et al. [26]. Since the mechanism from Yoo et al. [5] is the only one not exhibiting this multi-stage ignition, and in order to do a reliable comparison with the DNS study, the 88 species mechanism from [5] is the one extensively evaluated in this work. The other ones are considered only for comparison in terms of the sensitivity to the reaction chemistry. Figure 1 also shows the results obtained for the detailed chemistry of Curran et al. [28] and Seidel et al. [29] for comparison, i.e. the base chemistry for the three before mentioned reduced mechanisms. The reader should note that the mechanism from [5] used in this work is the one with 88 species, in contrast to the further simplified 58 species (and 763 reactions) mechanism used in the DNS. The species bundling and Quasi-Steady-State Approximation (QSSA) technique used in the DNS for the simplification of the 88 species mechanism is avoided in this study in order to work with a more complex chemistry, and due to temporarily non-resolved issues regarding the implementation of the QSSA Fortran subroutine of the original 58 species mechanism into the C++ ODT environment using Cantera. The results are expected to be the same as in the original DNS, since the number of chemical reactions is maintained.

The final pre-selected chemical mechanisms and the original DNS chemical reaction mechanism are summarized in Table 2 with some of their distinctive characteristics.

4. Results

4.1. Sensitivity to initial conditions and ensemble statistics

The main focus of this work is to compare ODT 1D results to DNS data by Yoo et al. [5]. These results correspond to 2-D DNS and might be quantitatively different to 3-D behavior (as discussed in [6]). This implies some degree of compromise when comparing with ODT results, since ODT models a full 3-D turbulent field. However, to the best of the authors' knowledge, there is no DNS up to this date that has been able to simulate the complex chemistry of n-Heptane in a full 3-D turbulent field.

Figure 2 shows the reference case selected for the preliminary laminar evaluation with initial conditions specified according to Section 3.1. The temporal average behavior of the heat release rate and pressure are shown. Since the characteristic turbulent decay nature of the flow is the interesting property to be evaluated for this work, all of the averages done for the autoignition simulations presented in this paper follow a spatial averaging philosophy. Figure 2 is a representation of this spatial averaging, and also of a series of $N = 60$ ensemble members average. A sample size of $N = 60$ ensemble members was selected for all of the simulations in this work, since this was the minimum number of ensemble members to achieve an invariant shape of the mean spatial averages of heat release rate and pressure. The standard deviation σ shown in Fig. 2 corresponds to the degree of dispersion between ensemble members, thus it is a representation of the significant changes introduced by the different initial conditions due to the random initial temperature and velocity fields. The shape of the standard deviation of the sample is shown exemplary here. The large dispersion between the ensemble members, however, will be analyzed again in the context of the ODT model calibration. We note that, if the same initial conditions are used, $\sigma = 0$ in the laminar runs. We use the notation $<$1-D Laminar$>$ in Fig. 2 to refer to

Table 2
Preselected chemical mechanisms used in this study. The DNS 58 species chemical mechanism is listed as a reference only.

Author / Study	# Species	# Reactions	Description
Seidel et al. [26] (S56)	56 Species	198 Reactions	Skeletal Scheme from [29] reduced for very lean mixtures
Yoo et al. [5] (Y88)	88 Species	763 Reactions	Skeletal scheme obtained from applying two-stage Directed Relation Graph (DRG) and DRG-aided sensitivity analysis to detailed mechanism [28]
Yoo et al. [5] (DNS Mech., Y58)	58 Species	763 Reactions	Linearized QSSA and diffusive species bundling applied to previous 88 species skeletal scheme, without altering the number of reactions
Zhong and Zheng [27] (Z52)	52 Species	234 Reactions	Mechanism for three-component fuel. n-Heptane chemistry obtained from sensitivity analysis done to 188 skeletal scheme, obtained from two-stage Directed Relation Graph (DRG) applied to detailed mechanism [28]

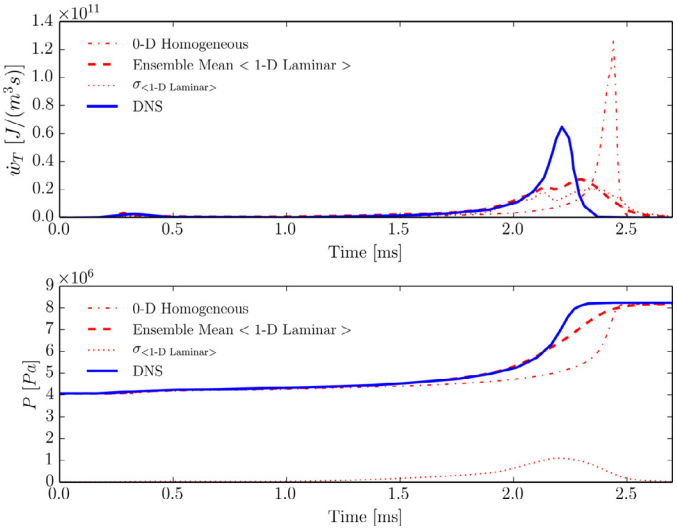

Fig. 2. Mean spatial behavior of the ensemble heat release rate (top) and pressure (bottom) as a function of time. Ensemble spatial-mean ODT result (red dashed) is compared to DNS spatial-mean data (blue solid) from [5]. For reference, ODT 0-D homogeneous reactor (red dashdot) and ODT laminar (red dotted) results are shown ($\Phi = 0.3$, $T_0 = 934$ K and $P_0 = 40$ atm). (For interpretation of the references to color in this figure legend, the reader is referred to the web version of this article.)

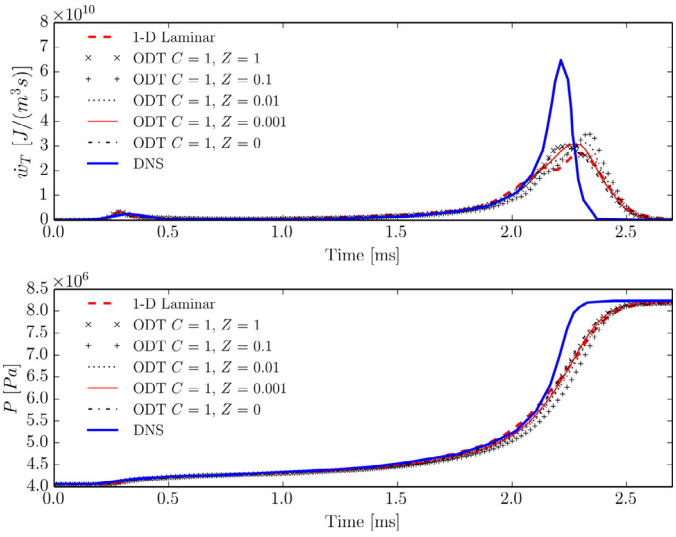

Fig. 3. Influence of ODT Z Parameter on mean spatial ensemble heat release rate (top) and pressure (bottom) as a function of time. For reference, ODT laminar results and DNS spatial-mean data are shown.

the ensemble and spatial averaged results. In the rest of the Figures in this work, for simplicity, we only use the notation 1-*D Laminar* for these averages (or *ODT* for turbulent simulations considering also this averaging philosophy).

The sensitivity of the constant volume autoignition flows to random initial conditions was already discussed in [8] (in the context of LEM). Such sensitivity motivated the series of DNS papers, among which the work of Yoo et al. [5] can be found. The initial temperature field distribution has a strong influence on the overall transient development of the flow conditions before ignition and this can already be seen in laminar flow conditions. The laminar flow is interpreted in this work as the absence of eddy events in the ODT model.

It is important to note that the DNS results from [5] shown in Fig. 2, and all of the figures including DNS results in this work, did not consider an ensemble statistical evaluation, but were rather the result of a one-time initialization of a certain turbulent (and temperature) field. This is justified and defined in the DNS study by following the same methodology as the study for hydrogen/air autoignition done by Hawkes et al. [3], where the authors used an identical initial temperature fluctuation field for all of the different temperature fluctuation amplitudes evaluated. The temperature field was just scaled by the appropriate amount according to the specified amplitude of the temperature fluctuations in each case. This is not the methodology used for this work. Here, each ensemble member (that could be interpreted as a different DNS realization) was initialized with a different random temperature field that preserved a given temperature fluctuation amplitude.

4.2. Sensitivity to ODT model calibration parameters

The ODT model calibration is achieved by determining the optimal values for C and Z to be used in Eq. (11) (parameters affecting the eddy acceptance probability).

Figure 3 shows the behavior of the mean spatial heat release rate and pressure over time for different values of the Z parameter at a fixed C parameter value ($C = 1$) in the ODT model, while Fig. 4 shows the same plots for different values of the C parameter at a fixed Z ($Z = 0.001$). In this work, a range of parameters of $1 \leq C \leq 10$ and $0 \leq Z \leq 1$ were selected based on the previous ODT explorations for variable density formulations in the case of Rayleigh–Taylor instabilities done by Gonzalez et al. [13] and the ODT formulation done by Jozefik et al. [14]. Note that C can take any desired value, but, as it was stated before, Z is an order-unity parameter in the model. Z is a viscous penalty parameter for the smallest length-scales, which, if used between the values $0 \leq Z \leq 1$, has only efficiency purposes. Considering values of $Z > 1$ would imply neglecting eddies larger than the Kolmogorov length scale.

It is clearly seen from Figs. 3 and 4 that both C and Z have very little influence on the behavior of the ensemble averaged heat release and pressure. This marginal influence might be attributed to the low turbulent Reynolds number of the reference case ($Re_t \sim 220$). The spatial and ensemble average of the pressure over time in Fig. 4 exhibits a shift towards a delayed second-stage ignition for increasing values of C. This coincides with the fact that an increased turbulence level quickly homogenizes the initial inhomogeneous temperature field and displaces the entire system behavior towards that of the 0-D homogeneous ignition.

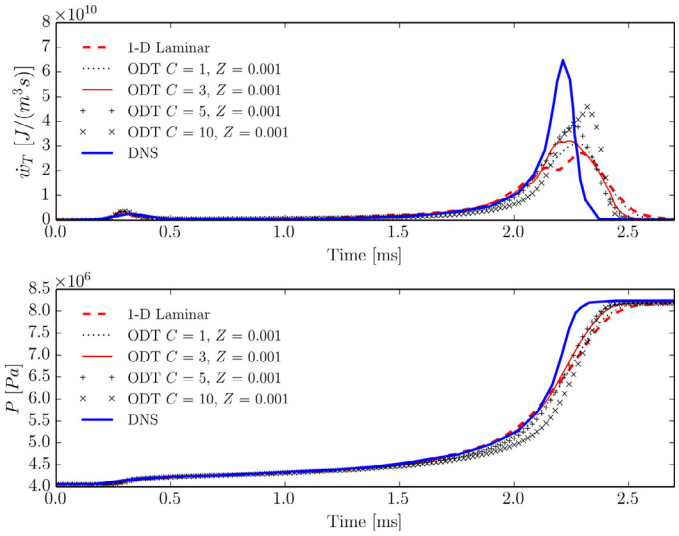

Fig. 4. Influence of ODT C Parameter on mean spatial ensemble heat release rate (top) and pressure (bottom) as a function of time. For reference, ODT laminar results and DNS spatial-mean data are shown.

Table 3
Criteria for the selection of optimal ODT parameters C and Z (Simulations with $\Phi = 0.3$, $T_0 = 934$ K, $P_0 = 40$ atm with initial temperature fluctuations $T' = 60$ K).

Parameters	**tpeakHRR, ODT** (s)	**HR until $t_{peakHRR,\ DNS}$ (J/m^3)**
$C = 1$, $Z = 0.001$	2.28	7.445×10^9
$C = 3$, $Z = 0.001$	2.24	8.054×10^9
$C = 5$, $Z = 0.001$	2.26	7.692×10^9
$C = 10$, $Z = 0.001$	2.32	6.223×10^9
$C = 1$, $Z = 0.01$	2.32	7.108×10^9
$C = 1$, $Z = 0.1$	2.34	6.291×10^9
$C = 1$, $Z = 1$	2.24	7.624×10^9
$C = 1$, $Z = 0$	2.26	7.832×10^9

Even though the comparison between the DNS results (for just one certain random initial temperature field) with the ODT ensemble average results (product of a set of different randomized initial conditions) might not be completely accurate, we select the optimal values of C and Z based on this comparison. We use the peak heat release rate events for calibration purposes. The peak heat release rate events are defined here as a qualitative evaluation of both the quantitative results for the time of peak heat release rate events for the ODT ensemble average behavior ($t_{peakHRR,\ ODT}$) and the absolute chemical heat release in J/m^3 achieved until the moment of peak heat release rate event in the DNS results, i.e. the integral of the heat release rate over time until $t_{peakHRR,\ DNS}$. These results are reported in Table 3.

By direct inspection of the obtained plots concerning the influence of Z and C on the spatial mean ensemble behavior and having reviewed the data obtained in Table 3, it is seen that a slightly faster ignition can be obtained for values of Z that are either 0 or 1 (intermediate values delay the ignition time). Since selecting $Z = 1$ implies imposing an eddy cutoff filter right at the Kolmogorov length-scale, selecting $Z = 0$ seems a more reasonable choice for this parameter from the physical point of view. However, selecting $Z = 0$ might result in a non-optimal performance of the code, and the occurrence of occasional deadlocks due to the appearance of extremely small eddies. Due to this reason, we select a value of Z very close to 0 ($Z = 0.001$), which produces very similar results to $Z = 0$. Regarding the C parameter, small values of C are able to produce faster second-stage ignition processes. Thus, we select the value $C = 3$. Another interesting comparison concerning the effects of the C and Z parameters can be seen in Fig. 5, where the temporal TKE evolution is plotted. For the TKE, the Z parameter has no influence at all, while the C parameter clearly accelerates the TKE consumption.

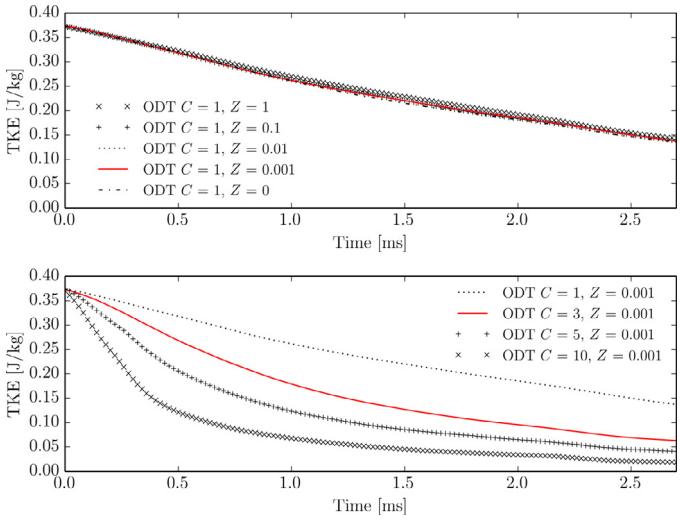

Fig. 5. Mean spatial ensemble ODT results for the TKE as a function of time. Top: influence of ODT Z parameter. Bottom: influence of ODT C parameter.

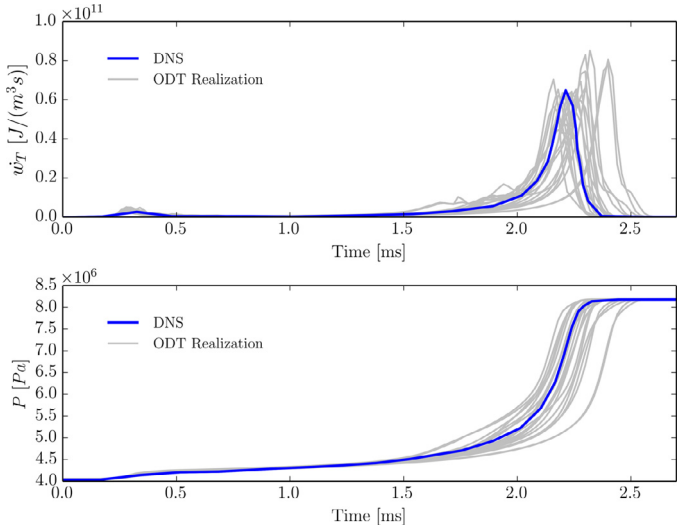

Fig. 6. Set of 20 ensemble members showing the mean spatial evolution for the heat release rate (top) and pressure (bottom). Each ODT realization (grey) has different initial conditions generated with Eq. (24) and uses the optimized C and Z parameters. DNS results are shown in blue for comparison. (For interpretation of the references to color in this figure legend, the reader is referred to the web version of this article.)

As it was commented before, the calibration process shown here is based on the comparison between specific DNS results and ensemble average ODT results, assuming that an ODT realization is equivalent to a DNS realization. In fact, the ODT average behavior (at least in the case of the Yoo et al. mechanism [5]) comprises a wide range of possible flow evolution scenarios, among which, the scenario of the DNS results can be observed. This is shown in Fig. 6, where 20 ensemble members are simultaneously plotted, some of them, coinciding with the DNS result.

To prove that for the case being studied here, an ODT realization is practically equivalent to a DNS realization, an additional set of $N_2 = 20$ ensemble members of ODT realizations corresponding to the initial conditions that were closest to DNS results within the original set of $N = 60$ ensemble members, is further presented in Fig. 7. In these realizations, the same initial conditions are

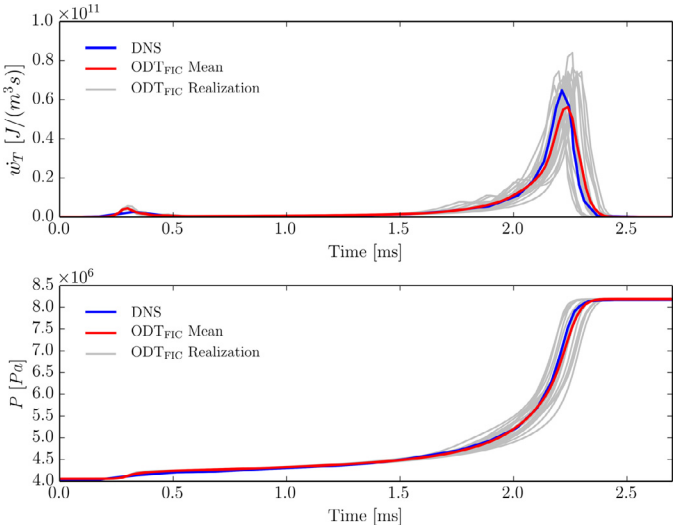

Fig. 7. Set of 20 ensemble members showing the mean spatial evolution for the heat release rate (top) and pressure (bottom). Each ODT realization (grey) used the optimized C and Z parameters and the same initial conditions, corresponding to the best-fit-to-DNS ODT results within the $N = 60$ ensemble members. The ODT random number seed was however varied. For reference, the $N_2 = 20$ ensemble average behavior (red) and DNS results (blue) are shown.(For interpretation of the references to color in this figure legend, the reader is referred to the web version of this article.)

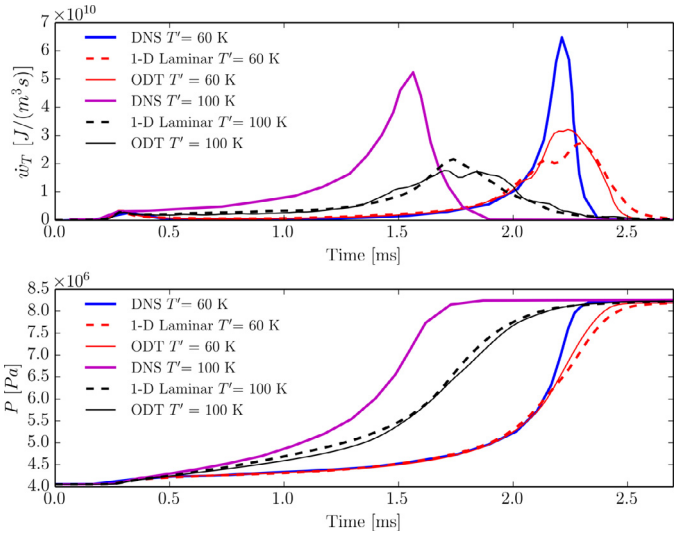

Fig. 8. Influence of initial RMS T' on the mean spatial ensemble heat release rate (top) and pressure (bottom) as a function of time. ODT results are compared to the equivalent DNS spatial-mean data. Laminar results are also shown for reference. (For interpretation of the references to color in this figure legend, the reader is referred to the web version of this article.)

considered, but the temporal evolution of the flow differs due to the different results in the stochastic eddy sampling and selection procedure. Figure 7 could then be interpreted as a measure of the degree of uncertainty inherent to the ODT stochastic model. By direct comparison of Figs. 6 and 7, it is possible to see that the outcome for the uncertainty of the model is marginal in comparison to the influence of the different initial temperature fields for the simulated cases, thus the flow evolution is dominated by the chemical initial conditions. Furthermore, each ensemble member in N, by itself, could be considered representative of a different DNS realization.

4.3. Influence of the magnitude of the initial temperature fluctuations

Due to the excessive dependence on the initial conditions, the next important parameter to evaluate is the amplitude of the temperature fluctuations in the initial inhomogeneous temperature field. To that extent, the $T' = 60$ K evaluated so far is compared in this section to the $T' = 100$ K results and both of these results are compared with the DNS data [5].

Figure 8 shows the temporally evolving ensemble averages of the mean spatial heat release rate and pressure. Increasing the amplitude of the temperature fluctuations in the starting inhomogeneous temperature field can be seen to accelerate the occurrence of peak heat release rate events and also to broaden the heat release dome. The broadening of the average heat release dome is also partly due to the increased dispersion between ensemble members. This can be seen in Fig. 9, by means of the representative standard deviation (σ) for the $N = 60$ ensemble with randomized initial conditions produced with Eq. (24), and the standard deviation for the $N_2 = 20$ ensemble that considers a given, fixed initial condition.

Although in this case it is clear that the displacement of the heat release dome corresponds to an earlier second-stage ignition, it is possible to confirm this hypothesis by examining the behavior of the density-weighted displacement speed S_d. Following the DNS methodology, an ignition front is tracked applying the definition of a density-weighted displacement speed. If such displacement speed is constant and close to a finite propagation reference speed (here, the laminar burning velocity), as suggested in the work done by Williams [30], then the regime is said to be a characteristical deflagration regime. Otherwise, if this displacement speed greatly exceeds this reference value by orders of magnitude, then the regime is said to be a characteristical detonation. The density weighted-displacement speed is defined in [5] as:

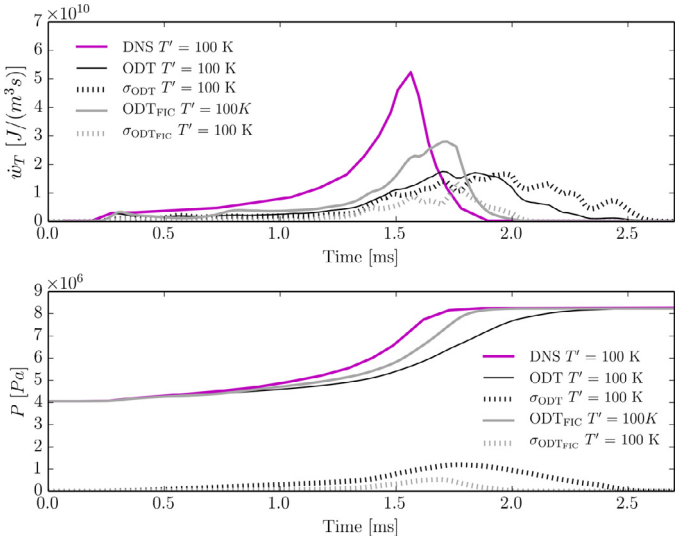

Fig. 9. Influence of using randomized initial conditions or Fixed Initial Conditions (FIC) on the mean spatial heat release rate (top) and pressure (bottom) as a function of time for the case with initial RMS $T' = 100$ K. Standard deviations obtained for the $N = 60$ ensemble with randomized initial conditions and $N_2 = 20$ ensemble with FIC are shown as reference.

$$S_d = \frac{\rho}{\rho_u}\left(\frac{1}{|\nabla Y_C|}\frac{DY_C}{Dt}\right)\Big|_{Y_C = Y_{C(\dot{w}_{T,peak})}}, \tag{26}$$

where ρ_u is a reference density for the unburnt state of the products, calculated by means of the local enthalpy and an assumed initial constant pressure P_0 and composition $Y_{k,0}$. Likewise, Y_C is defined as the mass fraction of the bundled diffusive species C, which is formed by $Y_C = Y_{CO_2} + Y_{CO}$. This chemical species tracks

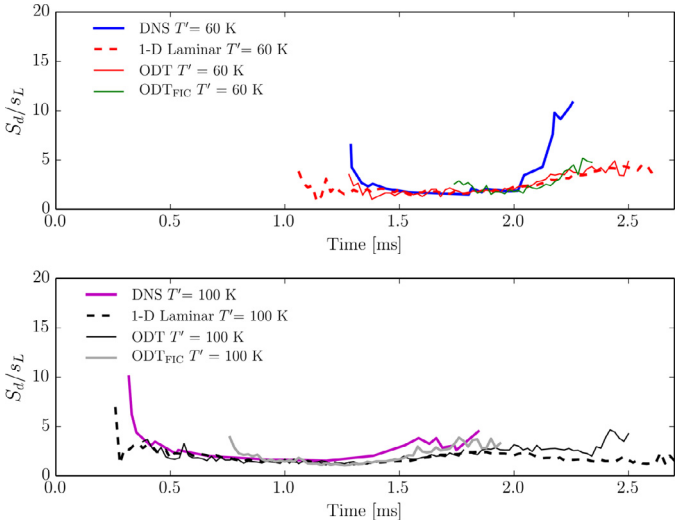

Fig. 10. Influence of initial RMS T' on the mean spatial ensemble normalized density-weighted displacement speed. ODT results considering randomized initial conditions and fixed initial conditions (FIC) are compared and evaluated to DNS results. Laminar results are also shown for reference. Top: $T' = 60$ K case. Bottom: $T' = 100$ K case. (For interpretation of the references to color in this figure legend, the reader is referred to the web version of this article.)

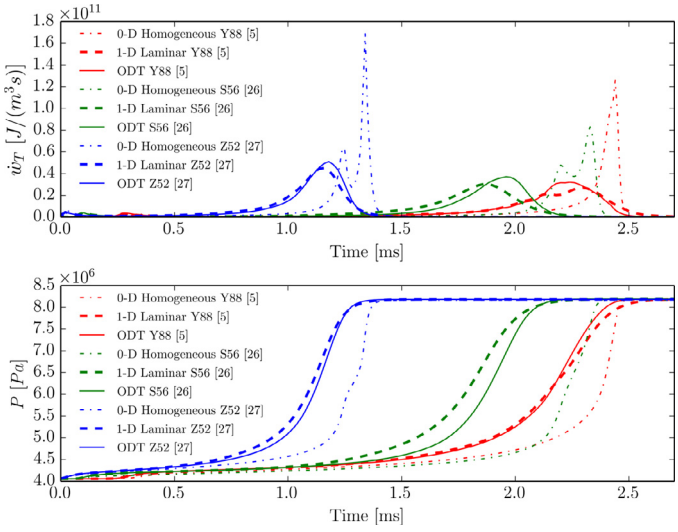

Fig. 11. Mean spatial ensemble heat release rate (top) and pressure (bottom) for the different mechanisms of [5], [26] and [27] as a function of time (Y88, S56 and Z52 refer to the mechanism identification according to Table 2). (For interpretation of the references to color in this figure legend, the reader is referred to the web version of this article.)

the ignition front. Since in this work, the mechanism used for evaluation is the one proposed by Yoo et al. [5] with 88 species (disregarding species bundling), some definitions of this species bundling method are required for the comparison with DNS results. To that extent, the mass fraction, reaction rate and mass diffusion coefficient of a species B composed of b bundled species, will be [31]

$$\begin{aligned} Y_B &= \sum_b Y_b, \\ \dot{w}_B &= \sum_b \dot{w}_b, \\ D_B &= D_b. \end{aligned} \tag{27}$$

Using the definition of the material derivative, and considering the Hirschfelder and Curtiss' approximation for species transport used in this work, Eq. (26) can be rewritten for a one-dimensional domain as

$$S_d = \frac{1}{\rho_u \left|\frac{\partial Y_C}{\partial x}\right|}\left[\frac{\partial(\rho D_C)}{\partial x}\frac{\partial Y_C}{\partial x} + \rho D_C \frac{\partial^2 Y_C}{\partial x^2} + \frac{\partial\left(\frac{\rho D_C Y_C}{M}\right)}{\partial x}\frac{\partial M}{\partial x} + \frac{\rho D_C Y_C}{M}\frac{\partial^2 M}{\partial x^2} + \dot{w}_C\right]. \tag{28}$$

All of the derivatives, mass diffusion coefficients, reaction rates, densities, among other properties, are evaluated for Y_C at the peak heat release rate $\dot{w}_{T,peak}$ in a 0-D homogeneous reactor, i.e. $Y_C = 0.04$. The right hand side of Eq. (28) is carefully discretized with a second order central difference scheme and a grid interpolation to the values with $Y_C = 0.04$ is used. Also, it is important to note that there might be more than one place along the domain where the desired value of Y_C appears, thus S_d is also the result of an ensemble averaging that includes all of these locations.

The behavior of the normalized density-weighted displacement speed can be seen in Fig. 10, where the ODT results for the case of $T' = 60$ K and $T' = 100$ K are shown. It can be seen in Fig. 10 that the reduced amplitude of the initial temperature fluctuations in combination with ODT reduces the spread of the heat release rate dome ($T' = 60$ K case). For the $T' = 100$ K case, a sustained flame front deflagration regime in the mean ensemble behavior can be obtained along practically the entire duration of the simulation. Note that the ignition is not instantaneous due to the large inhomogeneity of the system, thus the existence of the sustained deflagration regime. The existence of a flame front in the $T' = 100$ K case is far more likely than in the $T' = 60$ K case. In general, the mean ODT ensemble behavior is similar to the DNS representative results. Although it is not shown here, each one of the ODT ensemble members is able to capture the characteristic U-shape curve of S_d very well, and some ensemble members are also capable of achieving very close results to those of the DNS. In that sense, Fig. 10 also shows the influence on the normalized density-weighted displacement speed due to the use of randomized initial conditions against the selection of one fixed initial condition.

4.4. Variation of the chemical reaction mechanisms

As the last important topic of interest, the behavior of the heat release rate, pressure, density-weighted displacement speed and TKE are revisited from the perspective of the sensitivity of the results to the different chemical mechanisms (see Table 2). We assessed extensively already the mechanism of Yoo et al. [5] and now the mechanisms of Seidel et al. [26] and Zhong and Zheng [27] are considered.

In order to give some context before detailing the turbulent simulations, the 0-D homogeneous behavior and the laminar 1-D behavior are examined in Fig. 11 using $T' = 60$ K. The first important difference to note between the results obtained in 0-D homogeneous behavior by the skeletal mechanism of Yoo et al. [5] and the results obtained by the mechanisms from Seidel et al. [26] and Zhong and Zheng [27], is that the ignition process produced by the mechanisms of Seidel et al. [26] and Zhong and Zheng [27] does not occur in a one-step process with a single peak heat release, like it is seen in the results obtained with the skeletal mechanism of Yoo et al. [5]. Instead, a multi-step ignition process seems to take place (presence of 2 peaks on the temporal evolution of the mean spatial heat release rate). This multi-step ignition process in homogeneous conditions is not seen by the detailed mechanism from Seidel et al. [29] (not shown here for simplicity), which might be a reason to think that the chemistry introduced in the reduced mechanisms is somehow artificial in the evaluated conditions.

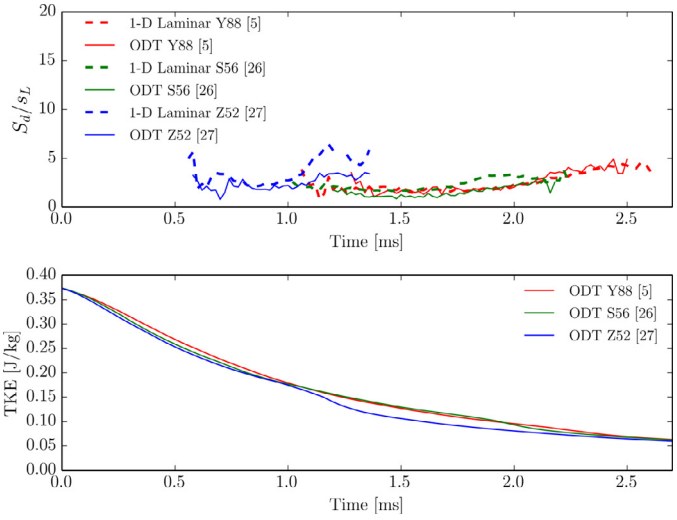

Fig. 12. Mean spatial ensemble normalized density-weighted displacement speed (top) and TKE (bottom) for the different mechanisms of [5], [26] and [27] as a function of time (Y88, S56 and Z52 refer to the mechanism identification according to Table 2). (For interpretation of the references to color in this figure legend, the reader is referred to the web version of this article.)

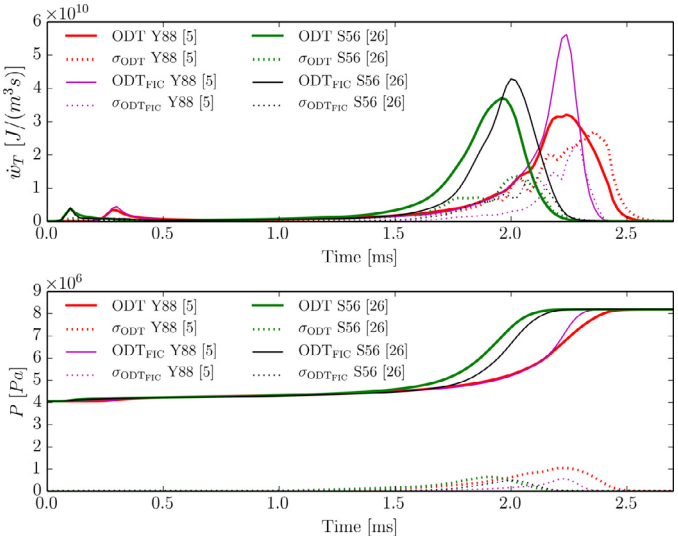

Fig. 13. Ensemble average and ensemble standard deviation evolution of the heat release rate and pressure for the difference chemical reaction mechanisms of [26] and [5]. The mean of different ODT realizations for Fixed Initial Conditions (FIC) closest-to-DNS results and its standard deviation (model uncertainty) are also shown for comparison (Case $T' = 60$ K). The notation Y88, S56 and Z52 refers to the mechanism identification according to Table 2. (For interpretation of the references to color in this figure legend, the reader is referred to the web version of this article.)

The different species present in the mechanisms produced different ignition delay times as it was seen in Fig. 1. This is seen now again in Fig. 11 with the relative position of the heat release rate domes associated to each mechanism. Another fact worth noting lies in the disappearance of the before mentioned multi-step ignition for the mechanisms of Seidel et al. [26] and Zhong and Zheng [27] when the initial temperature inhomogeneities are introduced (difference between 0-D and 1-D Laminar behavior).

Figure 11 also shows the comparison between the behavior of the heat release rate and pressure using different chemical mechanisms for both the laminar flow and the turbulent flow. The results suggest that the marginal turbulence level does not play a role in the heat release rate nor in the pressure for the most reduced chemical mechanisms. The dominant cause of difference is then the reaction chemistry.

Even in the turbulent conditions, the mechanism from Zhong and Zheng [27] is the one that reaches the highest and fastest peak heat release rate. This is corroborated by the results shown in Fig. 12, where the ignition flame front appearance denoted by the appearance of the curve for the density-weighted displacement speed occurs earlier for the mechanism of Zhong and Zheng [27] in comparison to the mechanisms of Seidel et al. [26] and Yoo et al. [5]. The larger heat release rate produced by the reaction chemistry of Zhong and Zheng [27] also provokes a slightly larger drop in the TKE consumption, as it is shown in Fig. 12. Despite the earlier second-stage ignition achieved by the mechanisms from Seidel et al. [26] and Zhong and Zheng [27], all of the mechanisms exhibit a characteristic flame front deflagration regime during ignition.

The uncertainty of the ODT model is further quantified for the different chemical reaction mechanisms. Figure 13 shows the mean of the ODT realizations for the initial condition that was closest-to-DNS, $< ODT_{FIC} >$, i.e. the mean behavior obtained in Fig. 7. The figure also shows the mean ensemble behavior for randomized initial inhomogeneous temperature fields, $< ODT >$, for the mechanisms of Seidel et al. [26] and Yoo et al. [5]. The standard deviation is shown as well in Fig. 13, symbolizing the uncertainty of the ODT model for the case of the realizations with fixed initial conditions. Conversely, the standard deviation for the case of the mean ensemble behavior, symbolizes the degree of dispersion between the $N = 60$ ensemble members for randomized initializations, similar to the idea shown in Fig. 2, considering in this case the dispersion between ensemble members in Fig. 6. Although the standard deviations corresponding to heat release rates in Fig. 13 have not yet converged (more ensemble members would be needed), it is interesting to note the pressure behavior of both mechanisms. For both cases, the standard deviation due to randomized initializations remains much larger than the deviation owed to model uncertainty.

5. Conclusions

In this study we have shown how the ODT approach can be applied to simulate constant volume autoignition flows of premixed n-Heptane/air mixtures. In addition, different types of chemical mechanisms have been implemented and tested to study the effect of the turbulent and chemical interactions under the specified initial conditions.

For all the chemical mechanisms investigated, constant volume autoignition flow evolution depends strongly on the initial conditions and in particular on the magnitude of the initial temperature field inhomogeneities. Larger temperature fluctuations in the initial temperature field accelerate the second-stage ignition of the system, producing a more sustained deflagration regime. This confirms the results of the DNS [5].

Within the ODT model, an increased turbulence level given by a higher value of the model parameter C, produces a faster homogenization of the temperature field and shifts the system behavior to that of the 0-D homogeneous combustion. It was shown that the influence of the turbulence level was more important than the removal of length-scales smaller than the Kolmogorov scale for ODT constant volume autoignition systems (influence of C over Z on the results).

Ensemble average behavior is normally associated in temporally evolving ODT lines as the equivalent to DNS behavior. Due to the low turbulence of the cases studied here, we showed the dominance of the initial chemical conditions of the flow in comparison to the stochastic outcomes of the eddy sampling and selection. Also, due to this reason, one ensemble member in this work could be considered close to a DNS realization. We also showed that it is possible to produce ensemble statistics for a wide range of ini-

tial conditions, which was not done in the DNS due to the high computational cost associated to the simulations.

As an example of the computational savings achieved with ODT, the simulations presented in this work took no longer than 18 h for a single ensemble, which with a cluster of 40 processors in parallel allowed to compute the required number of 60 ensemble members in just 2 days. As it was discussed in the introductory section, the history of the study by Yoo et al. [5] comprised more than 6 years of chemistry mechanism reduction techniques among other compromises like restriction to 2-D combustion to yield feasible DNS. In this work, even though some degree of chemistry reduction was required, a more complex reaction chemistry was used thanks to the computational savings of the ODT model.

Declarations of interest

None.

Acknowledgments

The authors acknowledge the contributions, support and discussions provided to this work made by L. Seidel. Special recognition is given to M. Klein for his valuable contributions regarding the writing style and typographic corrections for this publication.

Appendix A. Evolution of the Lagrangian ODT velocities

An important point in the ODT constant volume autoignition formulation is the discussion regarding the role of the momentum evolution equation. ODT velocities do not advect fluid, and as such, they are in principle only considered as energy containers for the balance influencing the eddy sampling and selection procedure discussed in Section 2.2 [18].

The hydrodynamic pressure gradient term, which appears in the Navier–Stokes momentum conservation equation in the Zero-Mach limit approximation, is traditionally neglected in the ODT formulations. The $\partial P_2/\partial x$ term that would appear in the 1-D momentum equation (hydrodynamic pressure gradient taken along the resolved ODT domain direction) can be split into mean and fluctuation components. The mean component in this case, is responsible for the net advection of the flow, which is zero in the case of constant volume autoignition considered here. Conversely, the fluctuation component redistributes the available energy among the velocity components u_j and can be modeled within the quasi-incompressible eddy events. Formally, $\partial P_2/\partial x$ is therefore omitted in the governing equations and the stress tensor is replaced by the 1-D incompressible counterpart for consistency with quasi-incompressible turbulent advection treatment. Thus, Eq. (2) is obtained.

The splitting of the Lagrangian velocity vector in Eq. (13) is justified by the fact that the ODT velocity components are dynamically passive with respect to evolution by diffusive (and by extension, reactive) driven advection [19]. In other words, the ODT velocity components are passive with respect to the heat and species diffusion, as well as chemical reactions effects that conform with the velocity divergence applicable for the Zero-Mach number limit approximation. Also, since the ODT velocity components satisfy a zero-divergence velocity field, they are not responsible for changes in the size of the control volumes (cells), in contrast to the non-zero-divergence dilatational velocity field. Since ODT does not provide a mechanism for eddies to be influenced by dilatational flow, an additional model is required influencing the eddy selection process only, but which is already enforced in the overall diffusion–reaction conservation of the system due to the formal splitting of the velocity in Eq. (13). This is the reason behind the usage of the Darrieus–Landau instability model for this study, as it was previously introduced by Jozefik et al. [14].

Appendix B. Convergence analysis of the time-stepping scheme

In this section we perform a time convergence analysis in order to determine the overall accuracy of the employed time-stepping scheme. Since the system of equations governing the diffusion–reaction advancement comprises non-conservative variables (P, u_D, u_j, Y_k, h), conservation is expected to be limited to the truncation error of the governing equations, and therefore it is desirable to evaluate the equations with a high order precision scheme.

Although the periodic boundary conditions applied in this work should preserve the theoretical order of accuracy of the Strang-Splitting procedure, the reader is referred to the work of [32] for an interesting discussion regarding the issues of accuracy order reduction in diffusion–reaction splitting. Such issues were already commented in the first version of the work of Pember et al. [22].

Based on the idea of [21] and [22], we tried to fully advance Eqs. (3) and (4) with the Strang-Splitting method in this work. The convergence analysis done in this Appendix shows, however, that the evaluation of the order of accuracy of the scheme is not so straightforward as it is usually done in other studies. This is due to the presence of the implicit reaction integration done via a Newton Method iteration of a Backward Differentiation Formula (BDF) with CVODE [23]. The use of the CVODE solver in this work follows the same principle as the use of implicit integration in the diffusion part of the scheme, namely, the pursue of an unconditionally stable numerical scheme that counteracts the stiff chemistry effects. For an interesting discussion concerning error estimation in production codes, such as the one used in this work, the reader is referred to [33].

Figure 14 shows the error between numerical solutions for the space-averaged enthalpy, space-averaged n-Heptane mass fraction and pressure for the 56 species chemical mechanism in a laminar problem with $T' = 60$ K. The numerical solutions correspond to a time $t = 6.4 \times 10^{-5}$ s. Order accuracy between two points in Fig. 14 can be estimated by Eq. (B.1), where $\tilde{U}$ is an approximate solution and $p_{ref(\Delta t,\ \Delta t/2)}$ is an approximate order of accuracy or rate of convergence.

$$log_2\left(\frac{\left\|\tilde{U}_{\Delta t} - \tilde{U}_{\Delta t/2}\right\|}{\left\|\tilde{U}_{\Delta t/2} - \tilde{U}_{\Delta t/4}\right\|}\right) \approx p_{ref(\Delta t, \Delta t/2)}. \tag{B.1}$$

CVODE is a variable order and variable step-size linear multistep method that requires user-specified absolute and relative tolerances as an acceptance criteria for the predictor–corrector BDF scheme [23]. It is not part of the scope of this work to evaluate the accuracy or convergence of such linear multistep solvers. In this work, the absolute and relative tolerances for CVODE were set to 1.0×10^{-10} and 1.0×10^{-4}, respectively. For the reaction part of the splitting scheme, the error remains bounded even for non-smooth solutions, and as such, it is in principle not entirely possible to determine the order of accuracy of the scheme. CVODE can, however, determine the order of each one of the sub-steps taken during the integration. For very small time-steps, the differences between the predictor and corrector steps taken by CVODE might be so small, that a simple first order integration could satisfy the input tolerances, and this is precisely what the solver automatically does. For these cases, the second order accuracy of the reaction part of the scheme is not fulfilled. Using an explicit Euler method for the enthalpy advancement in the reaction part of the scheme is then, not an aggravating factor and does not worsen the overall order of accuracy. The formal requisite for an overall second order Strang-Splitting method is finally not met, due to the first order integration during the reaction part of the scheme. This could be

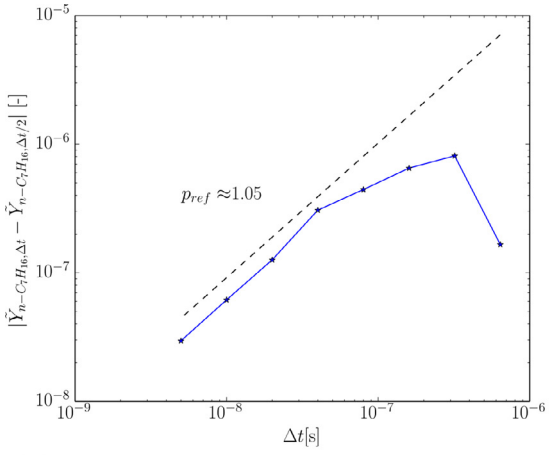

(a) Error behavior for $n - C_7H_{16}$ mass fraction

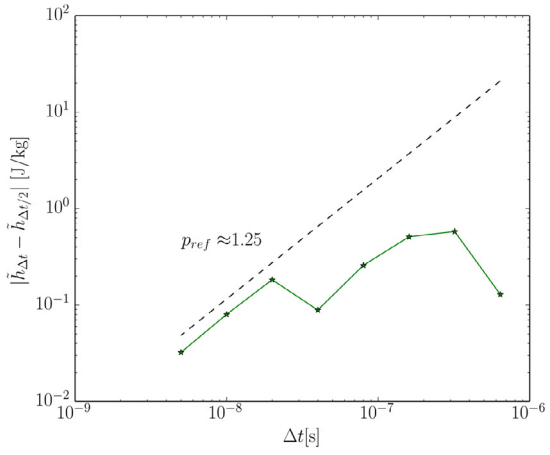

(b) Error behavior for enthalpy

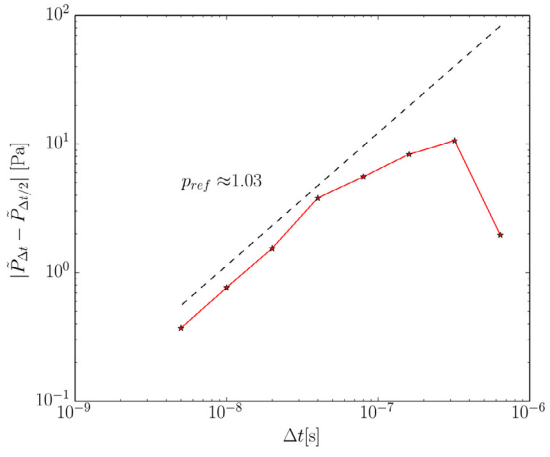

(c) Error behavior for pressure

Fig. 14. Error plots and reference orders of accuracy based on average slope.

the reason behind the collapse of the overall order of the scheme to first order.

Although one could argue that the resulting first order accuracy of the scheme does not justify the Crank–Nicolson and Runge–Kutta methods used for the diffusion advancement of the mass fractions and enthalpy, these schemes were only motivated due to stability reasons only, in order to be able to achieve larger time-steps magnitudes during the diffusion–reaction advancement.

As a closing comment the authors would like to stress that, regardless of the order of accuracy of the diffusion–reaction integration, all ODT simulations to date are first order in time due to the limitation of the stochastic transport part represented by the instantaneous eddy event implementation. Although a larger order of accuracy could be desired, this would need an additional splitting method for the turbulent transport in ODT. Such improvements might be analyzed in the future. It is nonetheless important to stress again, that ODT is a reduced order stochastic model which does not solve the generalized Navier–Stokes equations.

References

[1] S. Aceves, D. Flowers, C. Westbrook, J. Smith, W. Pitz, R. Dibble, M. Christensen, B. Johansson, A multi-zone model for prediction of HCCI combustion and emissions, SAE Technical Paper (2000-01-0327) (2000). doi:10.4271/2000-01-0327.

[2] J. Chen, E. Hawkes, R. Sankaran, S. Mason, H. Im, Direct numerical simulation of ignition front propagation in a constant volume with temperature inhomogeneities I. Fundamental analysis and diagnostics, Combust. Flame 145 (2006) 128–144.

[3] E. Hawkes, R. Sankaran, P. Pébay, J. Chen, Direct numerical simulation of ignition front propagation in a constant volume with temperature inhomogeneities II. Parametric study, Combust. Flame 145 (2006) 145–159.

[4] R. Sankaran, H. Im, E. Hawkes, J. Chen, The effects of non-uniform temperature distribution on the ignition of a lean homogeneous hydrogen–air mixture, Proc. Combust. Inst. Vol. 30 (2005) 875–882.

[5] C.S. Yoo, T. Lu, J. Chen, C. Law, Direct numerical simulations of ignition of a lean n-heptane/air mixture with temperature inhomogeneities at constant volume: parametric study, Combust. Flame 158 (2011) 1727–1741.

[6] R. Yu, X. Bai, Direct numerical simulation of lean hydrogen/air auto-ignition in a constant volume enclosure, Combust. Flame 160 (2013) 1706–1716.

[7] M. Luong, G. Yu, T. Lu, S. Chung, C.S. Yoo, Direct numerical simulations of ignition of a lean n-heptane/air mixture with temperature and composition inhomogeneities relevant to HCCI and SCCI combustion, Combust. Flame 162 (2015) 4566–4585.

[8] M. Oevermann, H. Schmidt, A. Kerstein, Investigation of autoignition under thermal stratification using linear eddy modeling, Combust. Flame 155 (2008) 370–379.

[9] A. Kerstein, One-dimensional turbulence: model formulation and application to homogeneous turbulence, shear flows, and buoyant stratified flows, J. Fluid Mech. 392 (1999) 277–334.

[10] Z. Jozefik, A. Kerstein, H. Schmidt, Towards a compressible reactive multiscale approach based on one-dimensional turbulence, Springer, Berlin, pp. 197–211. doi:10.1007/978-3-319-11967-0.

[11] Z. Jozefik, A. Kerstein, H. Schmidt, Simulation of shock–turbulence interaction in non-reactive flow and in turbulent deflagration and detonation regimes using one-dimensional turbulence, Combust. Flame 164 (2016) 53–67.

[12] A. Ricks, J. Hewson, A. Kerstein, J. Gore, S. Tieszen, W. Ashurst, A spatially developing one-dimensional turbulence (ODT) study of soot and enthalpy evolution in meter-scale buoyant turbulent flames, Combust. Sci. Technol. 182 (1) (2010) 60–101.

[13] E. Gonzalez, A. Kerstein, D. Lignell, Reactive Rayleigh–Taylor turbulent mixing: a one-dimensional-turbulence study, Geophys. Astrophys. Fluid Dyn. 107 (5) (2013) 506–525, doi:10.1080/03091929.2012.736504.

[14] Z. Jozefik, A. Kerstein, H. Schmidt, S. Lyra, H. Kolla, J. Chen, One-dimensional turbulence modeling of a turbulent counterflow flame with comparison to DNS, Combust. Flame 162 (2015) 2999–3015.

[15] D. Lignell, A. Kerstein, G. Sun, E. Monson, Mesh adaption for efficient multiscale implementation of One-Dimensional Turbulence, Theor. Comput. Fluid Dyn. 27 (3–4) (2013) 273–295, doi:10.1007/s00162-012-0267-9.

[16] A. Majda, Compressible fluid flow and systems of conservation laws in several space variables, 1st ed., Springer, 1984.

[17] V. Giovangigli, Convergent iterative methods for multicomponent diffusion, Impact Comput. Sci. Eng. 3 (3) (1991) 244–276, doi:10.1016/0899-8248(91)90010-R.

[18] A. Kerstein, W. Ashurst, S. Wunsch, V. Nilsen, One-dimensional turbulence: vector formulation and application to free-shear flows, J. Fluid Mech. 447 (2001) 85–109.

[19] W. Ashurst, A. Kerstein, One-dimensional turbulence: variable-density formulation and application to mixing layers, Phys. Fluids 17 (2005), doi:10.1063/1.1847413.

[20] E. Motheau, J. Abraham, A high-order numerical algorithm for DNS of low–Mach-number reactive flows with detailed chemistry and quasi-spectral accuracy, J. Comput. Phys. 313 (2016) 430–454.

[21] M. Oevermann, C. Paschereit, C. Schrödinger, Numerical studies on the impact of equivalence ratio oscillations on lean premixed flame characteristics and emissions, Springer, Berlin, 2014, doi:10.1007/978-3-319-11967-0.

[22] R. Pember, L. Howell, J. Bell, P. Colella, W. Crutchfield, A. Fiveland, A. Jessee, An adaptive projection method for unsteady, low Mach number combustion, Combust. Sci. Technol. 140 (1998) 123–168, doi:10.1080/00102209808915770.

[23] A. Hindmarsh, R. Serban, User documentation for CVODE v2.8.2 (SUNDIALS v2.6.2), Lawrence Livermore National Laboratory, 2015.

[24] D. Goodwin, Cantera C++ user's guide, California Institute of Technology, 2002.

[25] J. Herzler, L. Jerig, P. Roth, Shock tube study of the ignition of lean n-heptane/air mixtures at intermediate temperatures and high pressures, Proc. Combust. Inst. Vol. 30 (2005) 1147–1153, doi:10.1016/j.proci.2004.07.008.
[26] L. Seidel, C. Netzer, M. Hilbig, F. Mauss, C. Klauer, M. Pasternak, A. Mastrisciano, Systematic reduction of detailed chemical reaction mechanisms for engine applications, ASME 2016 Internal Combustion Engine Fall Technical Conference (ICEF2016-9304) (2016).
[27] B. Zhong, D. Zheng, Chemical kinetic mechanism of a three-component fuel composed of iso-octane/N-heptane/ethanol, Combust. Sci. Technol. 185 (4) (2013) 627–644, doi:10.1080/00102202.2012.739223.
[28] H. Curran, P. Gaffuri, W. Pitz, C. Westbrook, A comprehensive modeling study of n-heptane oxidation, Combust. Flame 114 (1–2) (1998) 149–177.
[29] L. Seidel, K. Moshammer, X. Wang, T. Zeuch, K. Kohse-Höinghaus, F. Mauß, Comprehensive kinetic modeling and experimental study of a fuel-rich, premixed n-heptane flame, Combust. Flame 162 (2015) 2045–2058.
[30] F. Williams, Combustion theory, 2nd ed., Perseus Books, 1985.
[31] T. Lu, C. Law, Strategies for mechanism reduction for large hydrocarbons: n-heptane, Combust. Flame 154 (2008) 153–163.
[32] L. Einkemmer, A. Ostermann, Overcoming order reduction in diffusion-reaction splitting. Part 1: Dirichlet boundary conditions, SIAM J. Sci. Comput. 37 (3) (2015) A1577–A1592.
[33] L. Shampine, Error estimation and control for ODEs, J. Sci. Comput. 25 (1–2) (2005) 3–16.